Original Article

Institution of MECHANICAL ENGINEERS
Journal of ENGINEERING TRIBOLOGY

Effect of cylinder de-activation on the tribological performance of compression ring conjunction

Proc IMechE Part J:
J Engineering Tribology
2017, Vol. 231(8) 997–1006

DOI: 10.1177/1350650116684985
journals.sagepub.com/home/pij
SAGE

SR Bewsher[1], R Turnbull[1], M Mohammadpour[1], R Rahmani[1], H Rahnejat[1], G Offner[2] and O Knaus[2]

Abstract

The paper presents transient thermal-mixed-hydrodynamics of piston compression ring–cylinder liner conjunction for a 4-cylinder 4-stroke gasoline engine during a part of the New European Drive Cycle (NEDC). Analyses are carried out with and without cylinder de-activation technology in order to investigate its effect upon the generated tribological conditions. In particular, the effect of cylinder deactivation upon frictional power loss is studied. The predictions show that overall power losses in the piston–ring cylinder system worsen by as much as 10% because of the increased combustion pressures and liner temperatures in the active cylinders of an engine operating under cylinder deactivation. This finding shows the down-side of this progressively employed technology, which otherwise is effective in terms of combustion efficiency with additional benefits for operation of catalytic converters. The expounded approach has not hitherto been reported in literature.

Keywords

Cylinder de-activation, piston compression ring conjunction, mixed regime of lubrication, friction, power loss

Date received: 2 August 2016; accepted: 11 November 2016

Introduction

The automotive industry is driven by the need to manufacture more efficient vehicles, with ever-stringent global emission directives and regulations to reduce the effects of greenhouse gases. Better fuel economy and reduced emissions are key motivation for increased efficiency in internal combustion (IC) engines.

Different technologies have been used to reduce emissions and improve fuel economy. These include variable valve actuation (VVA), turbo-charging, stop-start and cylinder de-activation (CDA). Although these technologies show potential for reducing emissions and fuel economy, they also promote certain undesired side-effects such as durability or increased frictional losses in some engine conjunctions, which are not often taken into account.

Frictional power losses typically account for 15–20% of the overall losses in an IC engine. These include the piston ring and piston skirt friction,[1] which are the major contributors with 40–50% of the frictional losses.[2] These can be affected by changing the working conditions with the introduction of the aforementioned new technologies. Uras et al.[3] showed that frictional losses increase under stop-start conditions such as that experienced in an urban drive cycle with modern vehicles. Mohammadpour et al.[4] investigated the effect of CDA on big end bearing performance. They found that although the overall fuel efficiency was improved, the bearing efficiency was reduced through increased overall frictional power loss. This was caused as the result of reduced minimum lubricant film thickness, which can lead to higher wear of components and generated contact temperatures.

CDA is particularly effective at low and partial engine loading such as in congested traffic and in urban driving.[5] This is represented by the urban driving section of the New European Driving Cycle (NEDC).[6] Thus, to improve fuel economy, many

[1]Wolfson School of Mechanical, Electrical and Manufacturing Engineering, Loughborough University, Loughborough, UK
[2]AVL List GMBH, Graz, Austria

Corresponding author:
SR Bewsher, Wolfson School of Mechanical, Electrical and Manufacturing Engineering, Loughborough University, Loughborough, UK.
Email: S.R.Bewsher@lboro.ac.uk

modern IC engines utilise CDA technology. With CDA the intake and exhaust valves of the deactivated cylinders are closed during the combustion cycle. This eliminates the pumping losses. On the other hand, in order to maintain the required output power, the combustion pressure is increased in the remaining active cylinders, which leads to higher combustion efficiency. Finally, the higher exhaust temperature as a result of CDA aid the effective functioning of the exhaust catalyst. A study conducted by Douglas et al.[7] simulated the effect of CDA on emissions and fuel economy, based upon the NEDC. It was found that efficiency can be improved, but only for specific parts of the fuel map. The report suggested that CDA can be utilised for 75% of time spent under NEDC, resulting in an estimated fuel consumption saving of 10%. The fuel consumption saving is also coupled with an estimated 28% reduction in the NOx emissions.

The effects of CDA on IC engine performance and friction was studied by Boretti and Scalco[8] for a selection of deactivated cylinders. Although it was concluded that CDA would improve fuel economy of both petrol and diesel engines by 30% and 20% respectively, their contribution was confined to an overview of the piston-connecting rod-crank subsystem, and did not specifically refer to the piston ring pack.

The compression ring's main function is to seal the combustion chamber and prevent leakage of gases into the crank-case and ingression of lubrication into the chamber. Therefore, the compression ring should conform well to the cylinder bore, thus resulting in increased friction. Baker et al.[9,10] showed that compression ring elastodynamic modal behaviour and conformance to the bore surface results in a disproportionate share of parasitic losses from such a small contact conjunction.

The current study focuses on the effect of CDA upon the piston compression ring-to-cylinder liner contact conjunction. The analysis is based on the combined transient solution of 2D Reynolds equation, lubricant rheological state equations and the Greenwood and Tripp's method[11,12] for boundary interactions. Viscous friction of a thin lubricant film and boundary friction resulting from any asperity interactions on the counter surfaces are predicted and frictional power loss evaluated. A 4-cylinder 4-stroke gasoline engine is considered in a snapshot within the NEDC. The ring–liner conjunction is analysed assuming a required engine power with and without CDA. In the case of CDA, the frictional performance of both the active and de-activated cylinders is considered. The frictional performance of the compression ring conjunction under transient mixed regime of lubrication with CDA has not previously been documented in literature.

Methodology

Hydrodynamics

The 2D Reynolds equation for a compressible piezo-viscous lubricant is

$$\frac{\partial}{\partial x}\left(\frac{\rho h^3}{6\eta}\frac{\partial p}{\partial x}\right)+\frac{\partial}{\partial y}\left(\frac{\rho h^3}{6\eta}\frac{\partial p}{\partial y}\right)=\frac{\partial(\rho U h)}{\partial x}+\frac{\partial(\rho V h)}{\partial y}+2\frac{\partial(\rho h)}{\partial t} \tag{1}$$

where, for the current analysis, any side-leakage of the lubricant in the lateral contact direction due to Couette flow (along the periphery of the cylinder bore) is ignored ($V=0$). This condition is valid for an assumed circumferentially symmetric film in the ring-bore conjunction.

Furthermore, no axial motion of the ring relative to the piston within its retaining groove is assumed. In practice, the ring moves between the lower and upper groove lands during the piston cycle. Inclusion of this feature is only essential when gas flow analysis is considered, which is not the focus of the current analysis. Therefore, the sliding speed of the compression ring is taken to be that of the piston[13]

$$U(\varphi)=-r\omega\sin\varphi\left\{1+\cos\varphi\left[\left(\frac{\ell}{r}\right)^2-\sin^2\varphi\right]^{-\frac{1}{2}}\right\} \tag{2}$$

For the axial x-direction of the contact, Reynolds (or Swift–Stieber)[14,15] outlet boundary conditions are used, which determines the lubricant film rupture location. A fully flooded inlet is assumed. The boundary conditions become

$$\begin{cases} p_{x=-b/2} = P_a \\ p_{x=x_c} = P_c \\ \left.\dfrac{\partial p}{\partial x}\right|_{x=x_c} = 0 \end{cases} \tag{3}$$

where P_a is the ring inlet pressure, which is assumed to be the crank-case pressure in the piston downstroke sense and the combustion chamber pressure in its upstroke sense. The cavitation pressure, P_c, is considered to be the same as the atmospheric pressure in this analysis. The position, $x=x_c$ denotes the lubricant film rupture point. The current model does not include any lubricant film reformation beyond the point of lubricant film rupture.

Lubricant rheology

The lubricant viscosity and density are affected by temperature and pressure. For viscosity,

the Roelands[16] equation is used, with the further development of the same by Houpert[17] yielding

$$\eta = \eta_0 e^{\alpha^* p} \tag{4}$$

where η is the dynamic viscosity of the lubricant at temperature T. Morris et al.[18] used an analytical control volume thermal mixing model to determine the temperature of the lubricant in passage through the contact. They showed that the lubricant temperature in the compression ring-liner conjunction closely follows that of the cylinder liner, with generated heat due to viscous shear heating accounting for less than 2% of the same. Therefore, in the current analysis the average temperature of the liner is used for the value of T. α^* is a function of both pressure and temperature, with T_0 being the reference or ambient temperature, thus[17]

$$\alpha^* p = [\ln \eta_0 + 9.67]\left\{\left(\frac{T-138}{T_0-138}\right)^{-S_0} \times \left[\left(1+\frac{p}{1.98\times 10^8}\right)^{Z}-1\right]\right\} \tag{5}$$

Values of Z and S_0 are obtained as[17]

$$Z = \frac{\alpha}{5.1 \times 10^9[\ln(\eta_0)+9.67]} \tag{6}$$

$$S_0 = \frac{\beta(T_0-138)}{\ln(\eta_0)+9.67} \tag{7}$$

Variations of lubricant density with pressure and temperature are obtained using the Dowson and Higginson equation[19]

$$\rho = \rho_0\left(1+\frac{0.6\times 10^{-9}p}{1+1.7\times 10^{-9}p}\right) \times \left[1-0.65\times 10^{-3}(T-T_0)\right] \tag{8}$$

Conjunctional geometry

In the current study the compression ring is considered to be rigid, thus not undergoing its in-plane radial, as well as out-of-plane twisting deformation. A study including these features was carried out by Baker et al.[9,10] The generated contact pressures are also insufficient to cause any localised contact deflection as shown by Bolander et al.[20] and Mishra et al.[21] Therefore, the lubricant film shape is a function of its instantaneous gap and the ring axial profile, h_s as

$$h(x,t) = h_m(t) + h_s(x) \tag{9}$$

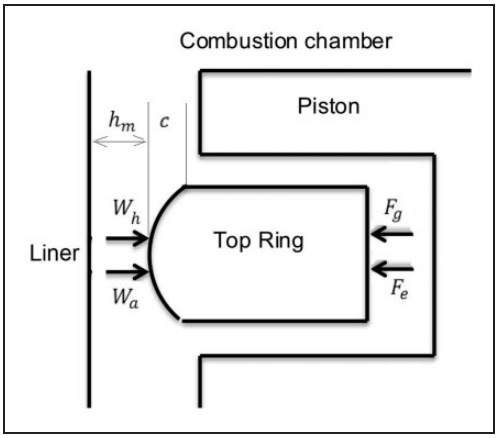

Figure 1. Radially applied forces acting on the compression ring.

$$h_s(x) = \frac{c(x-b/2)^2}{(b/2)^2} \tag{10}$$

Forces acting on the ring

Two outward forces act on the ring in its radial plane. These are the ring tension, F_e, and the gas force, F_g, which acts behind the inner rim of the ring (Figure 1). These forces strive to conform the ring to the cylinder liner surface, thus

$$F = F_e + F_g \tag{11}$$

where the gas force acting behind the inner rim of the ring is

$$F_g = p_g b l \tag{12}$$

p_g is found using the combustion pressure curve.

The ring tension force is

$$F_e = p_e b l \tag{13}$$

The elastic pressure is calculated using[22]

$$p_e = \frac{GE'I}{3\pi b r_0^4} \tag{14}$$

For a ring with an assumed rectangular cross section

$$I = \frac{1}{12} b d^3 \tag{15}$$

Rahmani et al.[22] considered an out-of-round cylinder where the compression ring only partially conforms to its surface in parts of the engine cycle. In the current analysis an idealised right circular cylinder is assumed, as in most studies reported in literature.

Transience of regime of lubrication

For parts of the engine cycle, particularly in the compression and power strokes at the piston dead centre reversals or in its immediate vicinity, analyses show prevalence of mixed or boundary regimes of lubrication.[20–25] Under these conditions, the mechanisms underlying generation of friction comprise viscous shear of a thin lubricant film, as well as direct interaction of asperities on the contacting surfaces. In fact, Styles et al.[26] showed that most of the generated friction in an engine cycle from the compression ring conjunction occurs in the vicinity of the top dead centre in transition from the compression to the power stroke. This prediction was in line with the observations made by Akalin and Newaz[27] using a motorised test rig, based on an engine cylinder and by Gore et al.[28] using a single-cylinder engine under both motorised and fired operating conditions with direct measurement of friction using a floating liner. Therefore, inclusion of a boundary friction model is an essential part of any representative analysis.

The applied load by ring tension and gas pressure on the ring is supported by the hydrodynamic reaction and the load share of asperities on the opposing surfaces. The hydrodynamic reaction is obtained as

$$W_h = \iint p \mathrm{d}x\mathrm{d}y \tag{16}$$

The load share of asperities is obtained using the Greenwood and Tripp[11,12] model, which assumes a Gaussian distribution of asperity heights with an average asperity tip radius of curvature, κ

$$W_a = \frac{16\sqrt{2}}{15}\pi(\zeta\kappa\sigma)^2\sqrt{\frac{\sigma}{K}}E'AF_{5/2}(\lambda) \tag{17}$$

$\zeta\kappa\sigma$, termed the roughness parameter, is found using topographical measurements; in this case using white light interferometry (Alicona infinite focus microscope) with a vertical resolution of 1 nm and a horizontal resolution of 0.175 μm with a focal magnification of $\times 80$. σ/κ is a measure of a typical asperity slope[29] and $\lambda = h/\sigma$ is the Stribeck's oil film parameter, with $1 \leqslant \lambda < 3$ taken as the region of mixed regime of lubrication, and $\lambda < 1$ corresponding to boundary regime of lubrication.

Therefore, the total load carried by the contact (contact reaction) is: $W = W_h + W_a$.

The use of Greenwood and Tripp[11,12] model implies a roughness profile of fairly smooth surfaces adherent to an idealised Gaussian distribution. In practice, cylinder liner surface is cross-hatched and honed and thus the topography deviates from an ideal Gaussian distribution. The Greenwood and Tripp model should therefore be adopted with measured topography to obtain a surface-specific non-Gaussian model as highlighted by Leighton et al.[30] Therefore, the use of a Gaussian distribution in the current study is for experimentally measured run-in liner topography.[22]

In the same manner, the total generated contact friction at any instant of time is

$$f = f_b + f_v \tag{18}$$

The boundary friction caused by the interaction of the opposing asperities is obtained as

$$f_b = \tau_0 A_a + \varsigma W_a \tag{19}$$

where ς is the shear strength of asperities on the softer of the two counter faces (in this case the cast iron liner). ς is analogous to the asperity-scale coefficient of friction and is measured using an atomic force microscope operating in lateral force mode. Styles et al.[26] described the procedure in detail. τ_0 is the Eyring shear stress of the lubricant,[31] in this case used for low to medium pressures and obtained through viscometry. Equation (19) also requires the determination of the area of asperity tips[11,12]

$$A_a = \pi^2(\zeta K\sigma)^2 AF_2(\lambda) \tag{20}$$

The viscous friction is calculated as

$$f_v = \int_0^l\int_0^b \tau \mathrm{d}x\mathrm{d}y \tag{21}$$

where the shear stress, τ is obtained as

$$\tau = \left| -\frac{\mathrm{d}p}{\mathrm{d}x}\frac{h}{2} + \frac{\eta U}{h} \right| \tag{22}$$

Method of solution

Reynolds equation has been discretised using a finite difference central method. A point successive over-relaxation method is then used to obtain the generated pressure distribution.[32] The iterative process is made up of the following steps:

1. An initial guess for the minimum film thickness is made at each crank angle, φ. This is used in equation (9) to find the film shape.
2. Using the film shape, a pressure distribution along the piston ring is calculated using the discretised Reynolds equation and lubricant rheological properties from equations (1), (4) and (6). Two convergence criteria must be satisfied.
3. The first criterion is for pressures, which is deemed to be converged when

$$Err_{pressure} = \frac{\sum_{i=1}^{I}\sum_{j=1}^{J}\left|p_{i,j}^{n} - p_{i,j}^{n-1}\right|}{\sum_{i=1}^{I}\sum_{j=1}^{J}p_{i,j}^{n}} \leqslant 1 \times 10^{-5} \tag{23}$$

If the criterion is not met, then over relaxation is applied

$$p_{i,j}^{n} = (1-\gamma)\, p_{i,j}^{n-1} + \gamma p_{i,j}^{n}; \qquad (0 < \gamma < 2) \tag{24}$$

The relaxation factor, γ, is determined by numerical testing. It was found that an over-relaxation factor of 1.4 yielded the fastest solution.

4. The second criterion is for load balance. The applied contact load, F, should equilibrate the contact reaction, W. Thus, at each crank angle

$$\left|\frac{W-F}{F}\right| \leqslant \varepsilon \tag{25}$$

where $\varepsilon \leqslant 10^{-3}$. In the current analysis, the convergence criteria is taken as: $\varepsilon = 10^{-5}$. When the equilibrium condition is not met the minimum film thickness is altered as

$$h_m^n = (1 + B\vartheta) h_m^{n-1} \tag{26}$$

where B is a damping coefficient with the value 0.01. ϑ is then calculated as

$$\vartheta = \frac{W-F}{max\{W,F\}} \tag{27}$$

5. When both convergence criteria are met, the crank angle is advanced within the combustion cycle, which for a 4-stroke process comprises 720°.

Validation of methodology

The numerical simulations described here use an existing and established CFD model.[33,34] These CFD models take into account the 3D solution of Navier–Stokes equation, but are computationally expensive. The input parameters from Tables 1 to 3 are used and the combustion curve in Shahmohamadi et al.[33] at an engine speed of 1500 r/min.[34] The results in Figure 2 show the minimum film thickness throughout the 720° engine cycle. It can be seen that there is a maximum deviation of 10% from the CFD results. This shows good agreement with the more detailed, but computationally intensive CFD model.[33]

Results and discussion

A C-segment vehicle with a 4-cylinder 4-stroke gasoline engine is used in the current analysis. The engine, lubricant, material and surface parameters are listed in Tables 1, 2 and 3, respectively. The engine speed is 1500 r/min. This speed corresponds to 35 km/h vehicle speed on the NEDC, when the car is driven in third gear. The delivered torque from the engine is 52.03 Nm.

The results presented are for conditions which all cylinders remain active, delivering the required torque. Results are also presented for CDA with two active cylinders delivering the same output torque. Figure 2 shows the combustion pressure, P_c, throughout the engine cycle. Figure 3 shows the

Table 1. Engine data.

Parameters	Values	Units
Torque	52.03	Nm
No. of cylinders	4	–
Engine type	Gasoline SI	–
Crank-pin radius, r	39.75	mm
Connecting rod length, l	138.1	mm
Bore nominal radius, r_0	44.52	mm
Ring crown height, c	10	μm
Ring axial face width, b	1.15	mm
Ring radial width, d	3.5	mm
Ring free end gap, g	10.5	mm

Table 2. Lubricant properties in atmospheric pressure.

Parameters	Values	Units
Lubricant viscosity, η_0	0.05 at 40°C0.009 at 100°C	kg/ms
Lubricant density, ρ_0	833.8 at 40°C799 at 100°C	kg/m^3
α_0	1 x 10^{-8}	m^2/N
Eyring shear stress, τ_0	2	MPa

Table 3. Material properties and surface topographical parameters.

Parameters	Values	Units
Liner material	Grey cast iron	–
Modulus elasticity of liner material	92.3	GPa
Poisson's ratio for liner material	0.211	–
Density for liner material	7200	kg/m^3
Ring material	Steel SAE 9254	–
Modulus elasticity of ring material	203	GPa
Poisson ratio for ring material	0.3	–
Roughness parameter $(\zeta \mathbf{K}\sigma)^{22}$	0.04	–
Measure of asperity gradient $(\sigma/\mathbf{K})^{22}$	0.001	–
Shear strength of asperities (ς)	0.17	–
Density for ring material	7700	kg/m^3

All topographical data in Rahmani et al.[22] were measured using white light interferometry with Alicona with measurement sensitivity of 1 nm normal to the surface and 0.175 μm in horizontal directions.

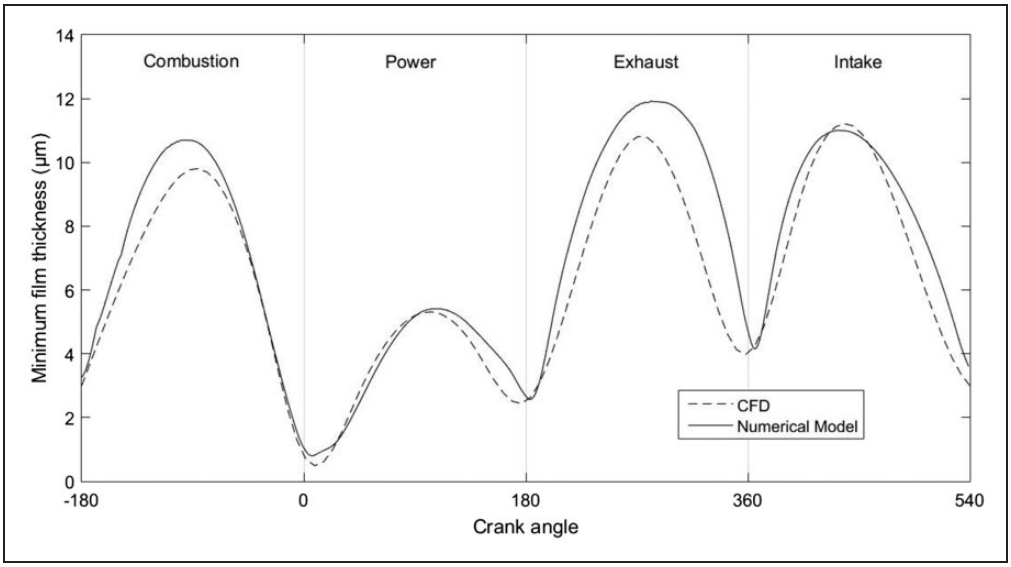

Figure 2. Minimum film thickness validation against CFD.[33,34]

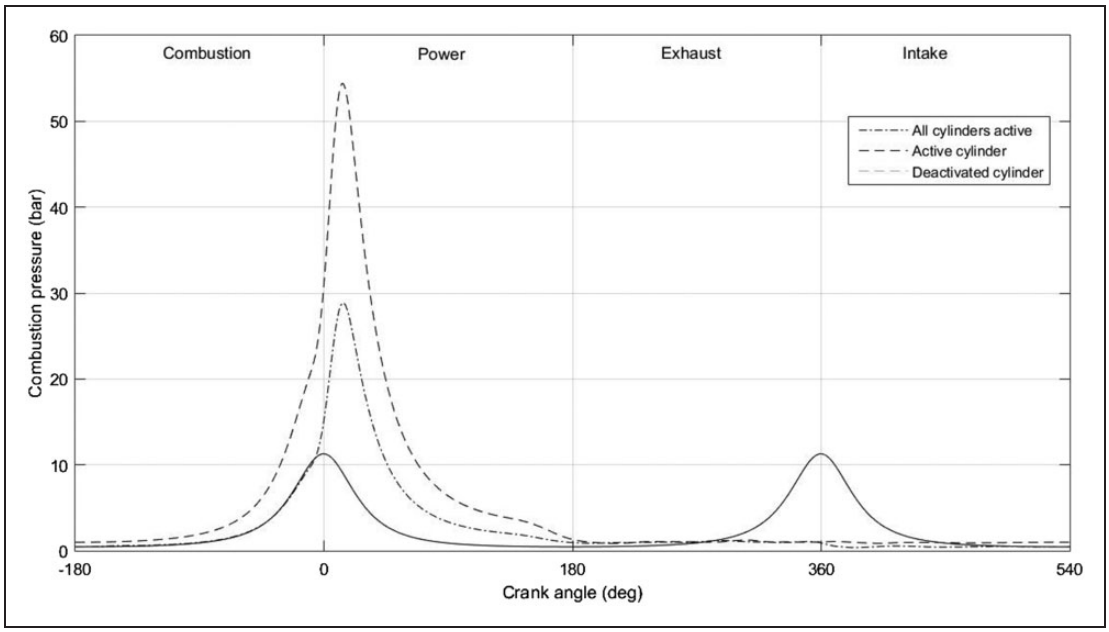

Figure 3. Combustion pressure.

corresponding measured variation in the liner temperature. The results correspond to (i) all active cylinders, (ii) an active cylinder in an engine with CDA and (iii) a deactivated cylinder in an engine with CDA.

The results are for the predicted minimum film thickness and the total friction in the piston top compression ring-to-cylinder liner conjunction. Under CDA, a considerable increase in the combustion pressure is required in the active cylinders to allow for the delivery of the same engine power as that with all the cylinder remaining active. In order to achieve this, a higher rate of fuel injection is required, which may not essentially achieve improved fuel efficiency and reduce engine emissions with CDA.

The crank angle $\theta = 0^\circ$ marks the position of the TDC at the onset of power stroke, with combustion occurring at 20° crank angle. For active cylinders during CDA, combustion occurs later. The maximum cylinder pressure for the deactivated cylinders occurs at the TDC. Pressure in deactivated cylinders results from entrapped air and any residual charge.

Figure 4 shows the equivalent liner temperature for each mode of operation. This is required in order to update the lubricant viscosity with the instantaneous in situ temperature.

Figure 5 shows the minimum film thickness in the piston ring to cylinder liner conjunction during the engine cycle. It can be seen that at TDC

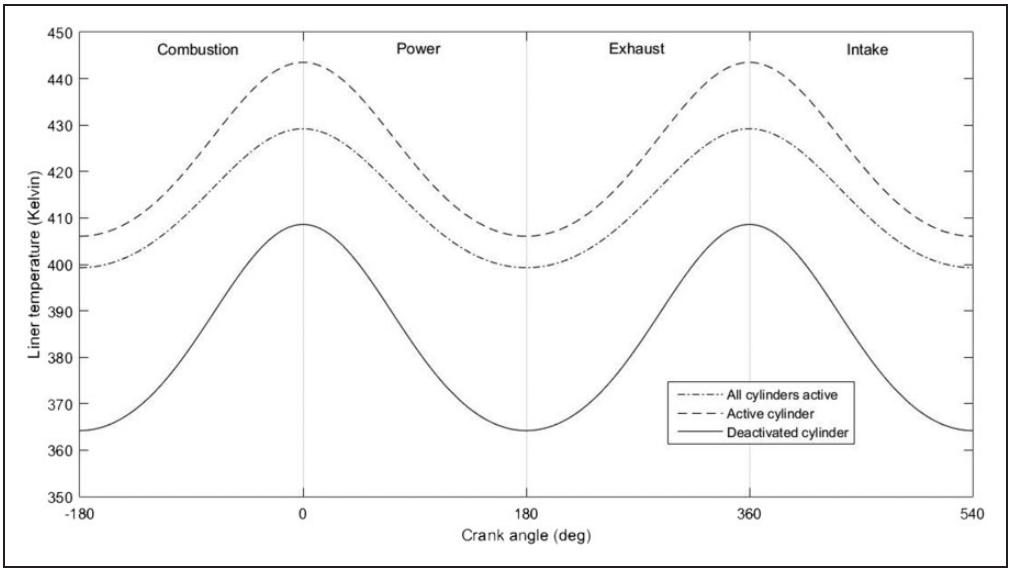

Figure 4. Liner temperature.

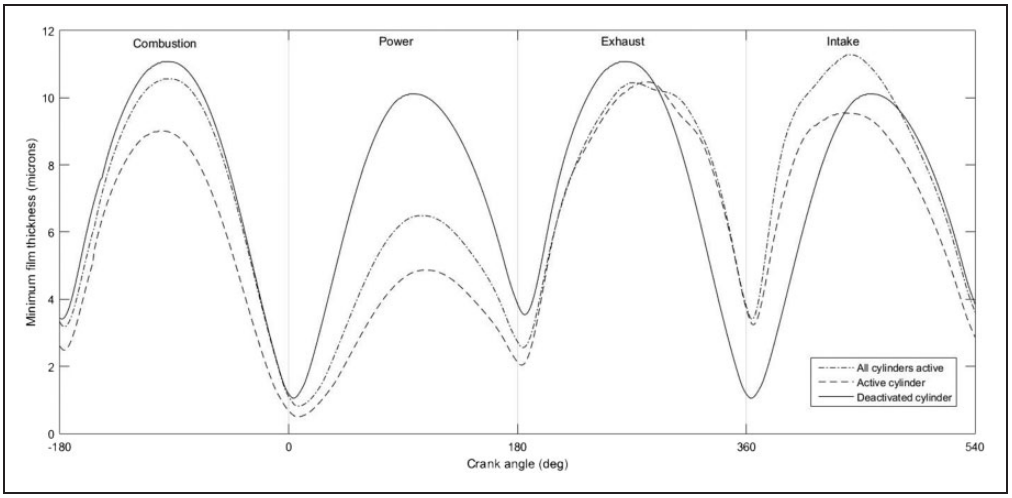

Figure 5. Cyclic variation of minimum film thickness.

($\varphi = 0^\circ$, 360°) the film thickness is reduced, with its minimum value occurring in the power stroke. As a result of the thinner film in the active cylinders of the engine, there are larger contributions to friction (Figure 6). For the activated cylinders, this is approximately double that experienced in a normal engine without CDA. However, for the deactivated cylinders it can be seen that there is a much lower predicted friction.

Analysing the results as a whole, it can be said that for multi-cylinder engines with CDA, frictional power losses are not necessarily reduced with the application of technology. The cause of this is the increased cylinder liner temperature in active cylinders at higher combustion (Figures 3 and 4).

In order to evaluate the effect of CDA on the overall efficiency of the system, the frictional power loss is calculated as

$$P_l = fU \tag{28}$$

Figure 7 shows the frictional power loss of compression ring under different conditions. The magnitude of frictional losses follows the friction variations in Figure 6. Table 4 shows the average power loss of each ring during the whole combustion cycle. This is 105.76 W for the engine without CDA, 116.9 W when CDA is used with two cylinders active. This amounts to a 9.53% increase in the overall power loss of compression rings with CDA. Therefore, although CDA is progressively utilised to improve combustion efficiency and catalyst performance, it has consequences in terms of tribological performance and frictional power loss.

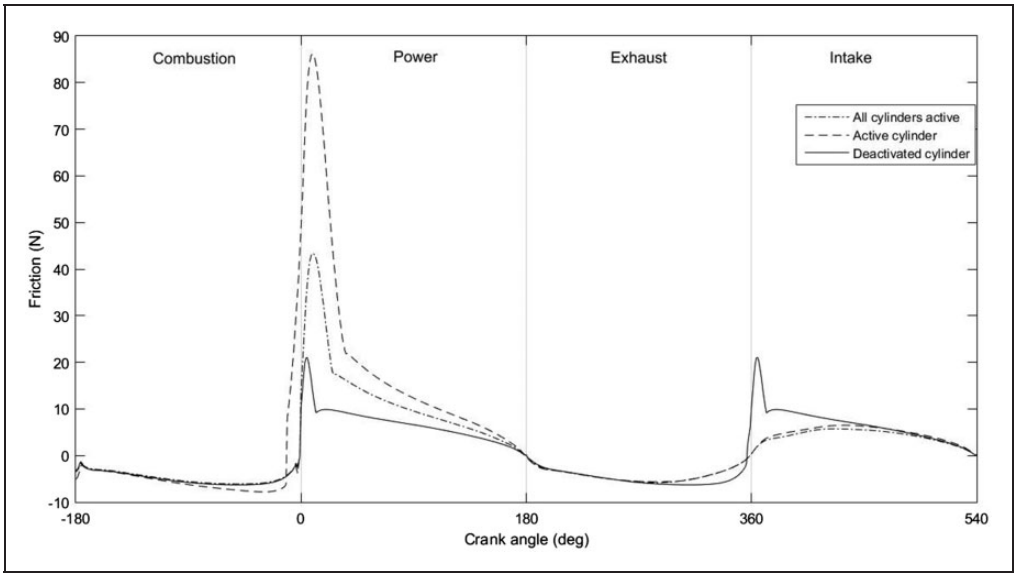

Figure 6. Cyclic total friction.

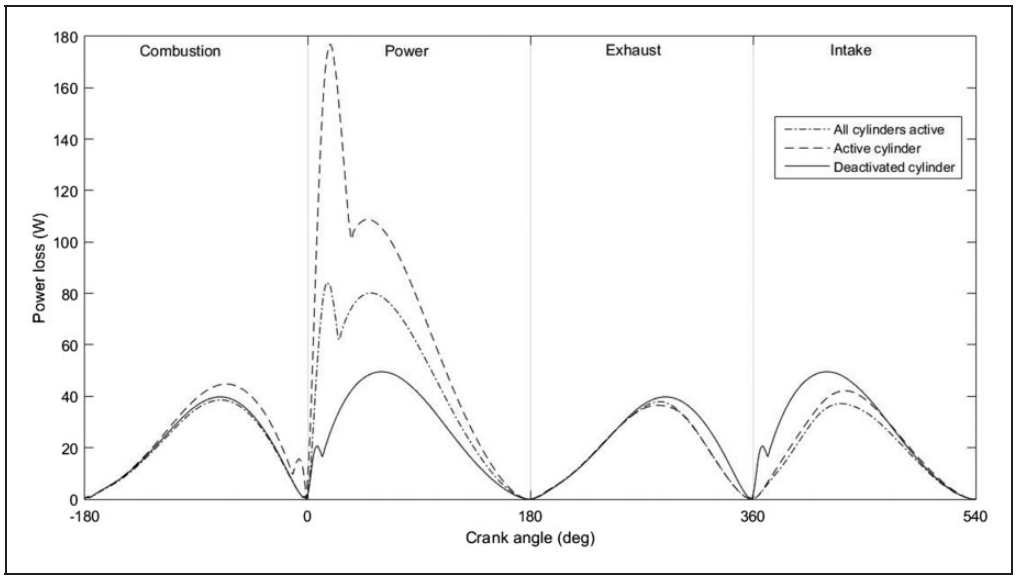

Figure 7. Frictional loss.

Table 4. Average frictional power loss of the compression ring.

	Average power loss (W) for each ring
All cylinders active	26.44
Active cylinder with CDA	33.87
Deactivated cylinder	24.58

Concluding remarks

This paper presents the effect of CDA on the tribological performance of piston ring to cylinder liner conjunction. The analysis shows that CDA has a significant effect on the film thickness and frictional power losses for the active and deactivated cylinders. It is shown that the total frictional loss in an engine with CDA is 9.53% higher than that in a similar engine under normal operational mode. Although the effect of CDA on frictional losses is not negligible, it is small in comparison with the higher gains (10%) in fuel economy because of higher combustion efficiency identified by Douglas et al.[7] The results of this paper indicated that the tribological consequences of this new technology should also be considered.

Declaration of Conflicting Interests

The author(s) declared no potential conflicts of interest with respect to the research, authorship, and/or publication of this article.

Funding

The author(s) disclosed receipt of the following financial support for the research, authorship, and/or publication of this article: The authors would like to thank the Engineering and Physical Sciences Research Council (EPSRC) for their funding, under which this research has been carried out in collaboration with AVL List who have also provided technical support.

References

1. Tung SC and McMillan ML. Automotive tribology overview of current advances and challenges for the future. *Tribol Int* 2004; 37: 517–536.
2. Fitzsimons B. Introduction to the importance of fuel efficiency and role of the Encyclopaedic research project. In: *IMechE seminar: A drive for fuel efficiency*, Loughborough, UK, 2011.
3. Uras H and Patterson DJ. Measurement of piston and ring assembly friction instantaneous IMEP method. SAE Technical Paper 830416, 1983.
4. Mohammadpour M, Rahmani R and Rahnejat H. Effect of cylinder de-activation on the tribo-dynamics and acoustic emission of overlay big end bearings. *Proc IMechE, Part K: J Multi-body Dynamics* 2014; 228: 135–151.
5. Falkowski A, McElwee M and Bonne M. Design and development of the Daimler Chrysler 5.7L HEMI® engine multi-displacement cylinder deactivation system. SAE Technical Paper, 2004 01-2106, 2004.
6. Eddington R. *The Eddington Transport Study: The case for action: Sir Rod Eddington's advice to government-December 2006*. Norwich, UK: HMSO: Department for Transport, 2006.
7. Douglas KJ, Milovanovic N, Turner JWG, et al. Fuel economy improvement using combined CAI and cylinder deactivation (CDA) - An initial study. SAE Technical Paper 2005-01-0110, 2005.
8. Boretti A and Scalco J. Piston ring and valve deactivation for improved part load performances of internal combustion engines. SAE Technical Paper 2011-01-0368, 2011.
9. Baker CE, Theodossiades S, Rahnejat H, et al. Influence of in-plane dynamics of thin compression rings on friction in internal combustion engines. *J Eng Gas Turbines Power* 2012; 134: 092801.
10. Baker C, Rahmani R, Theodossiades S, et al. On the effect of transient in-plane dynamics of the compression ring upon its tribological performance. *J Eng Gas Turbines Power* 2015; 137: 032512.
11. Greenwood JA and Tripp JH. The elastic contact of rough spheres. *J Appl Mech* 1967; 34: 153–159.
12. Greenwood JA and Tripp JH. The contact of two nominally flat rough surfaces. *Proc IMechE, Part C: J Mechanical Engineering Science* 1970; 185: 625–634.
13. Rahnejat H. *Multi-body dynamics: Vehicles, machines and mechanisms*. Bury St. Edmunds, UK: Professional Engineering Publishing, 1998.
14. Swift HW. The stability of lubricating films in journal bearings. *Proc Inst Civil Eng* 1932; 233: 267–288.
15. Steiber W. Das-Schwimmlager: Hydrodynamische Theorie des Gleitlagers. No. V.D.I., Berlin, 1933, p.106.
16. Roelands CJA. *Correlation aspects of viscosity-temperature-pressure relationships of lubricating oils*. PhD Thesis, Delft University of Technology, The Netherlands, 1966.
17. Houpert L. New results of traction force calculations in EHD contacts. *Trans ASME J Lubric Technol* 1985; 107: 241–248.
18. Morris N, Rahmani R, Rahnejat H, et al. Tribology of piston compression ring conjunction under transient thermal mixed regime of lubrication. *Tribol Int* 2013; 59: 248–258.
19. Dowson D and Higginson GR. *Elasto-hydrodynamic lubrication*. 2nd SI ed. Oxford, UK: Pergamon Press, 1977.
20. Bolander NW, Steenwyk BD, Sadeghi F, et al. Lubrication regime transitions at the piston ring-cylinder liner interface. *Proc IMechE, Part J: J Engineering Tribology* 2005; 219: 19–31.
21. Mishra PC, Balakrishnan S and Rahnejat H. Tribology of compression ring-to-cylinder contact at reversal. *Proc IMechE, Part J: J Engineering Tribology* 2008; 222: 815–826.
22. Rahmani R, Theodossiades S, Rahnejat H, et al. Transient elastohydrodynamic lubrication of rough new or worn piston compression ring conjunction with an out-of-round cylinder bore. *Proc IMechE, Part J: J Engineering Tribology* 2012; 226: 284–305.
23. Hu Y, Cheng HS, Arai T, et al. Numerical simulation of piston ring in mixed lubrication: A non-axi-symmetrical analysis. *Trans ASME J Tribology* 1994; 116: 470–478.
24. D'Agostino V and Senatore A. Fundamentals of lubrication and friction of piston ring contact. In: H Rahnejat (ed.) *Tribology and dynamics of engine and powertrain: Fundamentals, applications and future trends*. Cambridge, UK: Woodhead Publishing Ltd., 2010, pp.343–386.
25. Mishra PC, Rahnejat H and King PD. Tribology of the ring-bore conjunction subject to a mixed regime of lubrication. *Proc IMechE, Part C: J Mechanical Engineering Science* 2009; 223: 987–998.
26. Styles G, Rahmani R, Rahnejat H, et al. In-cycle and life-time friction transience in piston ring–liner conjunction under mixed regime of lubrication. *Int J Engine Res* 2014; 15: 862–876.
27. Akalin O and Newaz GM. Piston ring-cylinder bore friction modeling in mixed lubrication regime: Part II-Correlation with bench test data. *Trans ASME J Tribol* 2001; 123: 219–223.
28. Gore M, Theaker M, Howell-Smith S, et al. Direct measurement of piston friction of internal-combustion engines using the floating-liner principle. *Proc IMechE, Part D: J Automobile Engineering* 2014; 228: 344–354.
29. Gohar R and Rahnejat H. *Fundamentals of tribology*. London, UK: Imperial College Press, 2008.
30. Leighton M, Rahmani R and Rahnejat H. Surface-specific flow factors for prediction of friction of cross-hatched surfaces. *Surf Topogr: Metrol Prop* 2016; 4: 025002.
31. Eyring H. Viscosity, plasticity and diffusion as examples of absolute reaction rates. *J Chem Phys* 1936; 4: 283.
32. Hoffmann KA and Chiang ST. *Computational fluid dynamics for engineers - Volume 1*. Wichita, KS: Engineering Education System, 1993.
33. Shahmohamadi H, Rahmani R, Rahnejat H, et al. Thermo-mixed hydrodynamics of piston compression ring conjunction. *Tribol Lett* 2013; 51: 323–340.

34. Shahmohamadi H, Mohammadpour M, Rahmani R, et al. On the boundary conditions in multi-phase flow through the piston ring-cylinder liner conjunction. *Tribol Int* 2015; 90: 164–174.

Appendix

Notation

A	apparent contact area
A_a	asperity contact area
b	ring face-width
B	damping coefficient
c	ring crown height
d	ring radial width (thickness)
$Err_{pressure}$	convergence criteria for pressure
E'	composite reduced elastic modulus of the contacting pair
f	total generated contact friction
f_b	boundary friction
f_v	viscous friction
F	applied contact load
F_2	statistical function
$F_{5/2}$	statistical function
F_e	ring elastic force
F_g	gas force acting behind the ring rim
G	ring end gap
h	lubricant film thickness
h_m	minimum film thickness
h_s	axial profile of the ring
I	second moment of area
K	conformability coefficient (factor)
l	ring circumferential length or bore perimeter
ℓ	connecting rod length
n	iteration number
p	gauge pressure
P_e	ring elastic pressure due to fitment
P_g	gas pressure acting behind the inner ring rim
P_a	pressure at the ring inlet conjunction
P_c	combustion pressure
P_l	power loss
r	crank-pin radius
r_0	nominal bore radius
S_0	temperature-viscosity index
t	time
T	liner temperature
T_0	reference temperature
U	sliding velocity
V	lateral velocity (speed of side leakage flow)
W	total load carried by the contact
W_a	load share of asperities
W_h	hydrodynamic load
x	direction along the ring face-width
x_c	film rupture boundary
y	direction along the bore circumference
Z	pressure–viscosity index
α	pressure–viscosity coefficient
α^*	modified pressure–viscosity coefficient
β	temperature–viscosity coefficient
ε	limit of pressure convergence
η	lubricant dynamic viscosity
η_0	atmospheric dynamic viscosity
γ	relaxation factor
κ	average asperity tip radius of curvature
λ	Stribeck's oil film parameter
ω	engine speed
φ	crank angle
ρ	lubricant density
ρ_0	lubricant density at atmospheric pressure
σ	RMS composite surface roughness
ς	pressure coefficient of boundary shear strength of asperities
τ_0	Eyring shear stress
ϑ	load balance parameter
ζ	number of asperities per unit area of contact